Supporting information for

Ultrathin FeF_x Nanolayers Accelerating Hole Transfer for Enhanced Photoelectrochemical Water Oxidation

Chenchen Feng[a,b], Lei Wang[a], Shurong Fu[a,b], Kai Fan[a], Yajun Zhang[a] and Yingpu Bi*[a]

[a]State Key Laboratory for Oxo Synthesis & Selective Oxidation, National Engineering Research Center for Fine Petrochemical Intermediates, Lanzhou Institute of Chemical Physics, CAS, Lanzhou, Gansu 730000, China. E-mail: yingpubi@licp.cas.cn

[b]University of Chinese Academy of Sciences, Beijing 100049, China.

1. Experimental section

Preparation of Fe_2O_3 and Fe_2O_3-Pt nanoflake photoanodes:

The hematite electrodes were prepared by a simple impregnation method and middle temperature annealing at 400 °C.[1] In this work, we used Fe foils (Alfa Aesar, 99.99%) that were cleaned under sonication by sequentially immersing in acetone, ethanol for 10 min. The treated Fe foils (1×1 cm^2) were immersed in 5 mM H_2PtCl_6 (Sigma-Aldrich, 99.9%) aqueous solutions for 1 min to precipitate a Pt nanoparticles layer on the surface of Fe foils. Then, the Pt/Fe or Fe foils were thermally annealed in the furnace (HF-Kejing Furnace, KSL-1100X) in air at 400 °C, with ramping rate of 10 °C min^{-1}, kept at the desired temperature for 2h, and finally the samples were removed from the furnace. The samples were denoted Fe_2O_3 and Fe_2O_3-Pt.

Preparation of FeF_x/Fe_2O_3 and FeF_x-Fe_2O_3-Pt nanoflake photoanodes:

For in situ preparation of FeF_x/Fe_2O_3 nanoflake, the Fe_2O_3 or Fe_2O_3-Pt photoanodes were quickly dipped into a dilute hydrogen fluoride solution (0.02%, 0.1% and 0.5%), followed by rapid drying. Then, the samples were thermally annealed in the furnace (HF-Kejing Kurnace, KSL-1100X) in argon atmosphere at 250 °C for 4 h. The samples were denoted FeF_x-Fe_2O_3 and FeF_x-Fe_2O_3-Pt.

Preparation of FeOOH-Fe_2O_3-Pt nanoflake photoanodes:

The as-prepared photoanodes were immersed in the mixed precursor solution (45 mM urea and 30 mM $FeCl_3$) and kept in the oven at 100 °C for 10 min. After the deposition, the coated photoanodes were rinsed with deionized water, dried in 60 °C.

Preparation of pristine FeF_3 powders:

According to the previous reports,[2] 0.808 g $Fe(NO_3)_3{\cdot}_9H_2O$ was dissolved in 20 mL ethanol to result in a bright-orange solution of Fe^{3+}. 7.5 mL of ethanol and 2.0 mL of HF aqueous solution (48 w.t. %) were added into a 15 mL plastic centrifuge tube. The centrifuge tube was then sealed carefully and the mixture of two liquids was shaken to mix with great caution. This gave rises to a clear HF/ethanol solution, to which 0.5 mL Fe^{3+}/ethanol solution was quickly injected. The resulting colorless solution was shaken by hand and then heated in an oven at 60 °C for 24 h. The white cloudy precipitates that appeared over time were collected by centrifugation at a speed of 5000 rpm for 5 min, vigorously washed with ethanol twice and finally air dried at room temperature.

Finally, the FeF_3-Fe_2O_3-Pt nanoflake photoanodes were prepared by dripping 10 μL FeF_3 ethanol solution (2 mg/mL). After drying at room temperature, the samples were thermally annealed in the furnace in argon atmosphere at 250 °C for 4 h. The samples were denoted FeF_3-Fe_2O_3-Pt.

Preparation of Fe_2O_3-Pt photoanodes with dilute hydrochloric acid and Hydrobromic acid solution treatment.

At first, the dilute HCl and HBr aqueous solution have the same concentration with the above dilute HF aqueous solution. Similarly, the Fe_2O_3-Pt photoanodes were quickly dipped into the dilute hydrogen fluoride solution (0.1%), followed by rapid drying. Then, the samples were thermally annealed in the argon atmosphere at 250 °C for 4 h.

Characterization.

The X-ray diffraction spectra (XRD) measurements were performed on a Rigaku RINT-2000 instrument utilizing Cu Kα radiation (40 KV). The XRD patterns were recorded from 10° to 90° with a scanning rate of 0.067°/s. Scanning electron microscopy (SEM) measurements were carried out on a field-emission scanning electron microscope (JSM-6701F. JEOL) operated at an accelerating voltage of 5 KV. Transmission electron microscopy (TEM) measurements were carried out by using a FEI Tecnai TF20 microscope operated at 200 kV. UV-vis diffuse reflectance spectra were taken on an UV-2550 (Shimadzu) spectrometer by using $BaSO_4$ as the reference. The element composition was detected by X-ray photoelectron spectroscope (XPS, ESCALAB 250Xi).

Photoelectrochemical measurements.

The Photoelectrochemical properties were measured by an electrochemical analyzer (CHI660D) in a standard three-electrode system with the Fe_2O_3-based photoelectrodes (1×1 cm^2) serving as the working electrode (photoanode), a Pt foil as the counter electrode, and a saturated Ag/AgCl (4 M KCl) as a reference electrode. The illumination source was a 300 W Xe arc lamp (Beijing Perfectlight Technology Co. Ltd., Microsolar 300 UV) equipped with an AM 1.5G filter, and the power intensity of the incident light was calibrated to 100 mW/cm^2 at the surface of the working electrode. The current-voltage (*J-V*) characteristic of the electrodes, with a scan rate of 10 mV/s. A 1.0 M KOH aqueous solution (pH 13.6) was used as the electrolyte. All potentials of the working electrode were presented against the reversible hydrogen electrode (RHE).

$$E_{RHE} = E_{Ag/AgCl} + E_{Ag/AgCl}(reference) + 0.0591 \times pH$$

($E_{Ag/AgCl}$ (reference) = 0.1976 V vs. NHE at 25 °C)

Where pH is a pH value of the electrolyte.

The incident photon to current efficiency (IPCE) was determined using a full solar simulator (Newport, Model 9600, 300W Xe arc lamp) and motorized monochromator (Oriel Cornerstone 130 1/8 m). IPCE was measured at 1.23 V vs. RHE in 1.0 M KOH aqueous solution (pH 13.6) using the same three-electrode setup described above for photocurrent measurements. IPCE was calculated as follows:

$$IPCE(\%) = \frac{1240 \times I(mA/cm^2)}{P_{light}(mW/cm^2) \times \lambda(nm)} \times 100\%$$

Where I is the measured photocurrent density at a specific wavelength, λ is the wavelength of incident light and P_{light} is the measured light power density at that wavelength.

Supposing 100% Faradaic Efficiency, the solar-to-hydrogen (STH) efficiency was calculated by following equation:

$$STH(\%) = \frac{I(mA/cm^2) \times (1.23 - V_{bias})(V)}{P_{light}(mW/cm^2)} \times 100\%$$

Where I is the photocurrent density from the C-V curve shown in Figure 3A, V_{bias} (vs. RHE) is the applied bias between WE and RHE, P_{light} is the incident illumination power density (100 mW cm^{-2}).

The electrochemical impedance spectroscopy (EIS) Nyquist plots were measured in a 1.0 M KOH aqueous solution at 1.23 V (vs. RHE) with small AC amplitude of 10 mV in the frequency range of 0.1 to 10^5 Hz under AM 1.5G illumination (100 mW/cm^2). The measured spectra were fitted with Z-view software.

Detection of the amount of hydrogen and oxygen evolution:

To quantitatively determine the amount of H_2 and O_2 produced from the overall water splitting, an online gas analysis system (Labsolar 6A, Beijing Perfectlight Technology Co. Ltd.) and a gas chromatograph (GC 7890A, Agilent Technologies) were employed. The produce of H_2 and O_2 was performed in a three-electrode system at a constant bias of 1.23 V vs. RHE under AM 1.5G illumination (100 mW cm^{-2}).

The Faradaic efficiency was calculated by dividing the amount of gas detected by the theoretical amount of gas calculated on the basis of the total charge passed, using the following equation

$$FE(\%) = \frac{A \times n(mol) \times F(C/mol)}{Charge\ passed\ through\ WE(C)} \times 100$$

where n is moles of evolved H_2 or O_2 gas, A is the number of electrons required to generate one H_2 or O_2 molecule (two for H_2, four for O_2) and F is the Faraday constant (96485.33 C mol^{-1}).

2. Supplemental Figures and additional discussion

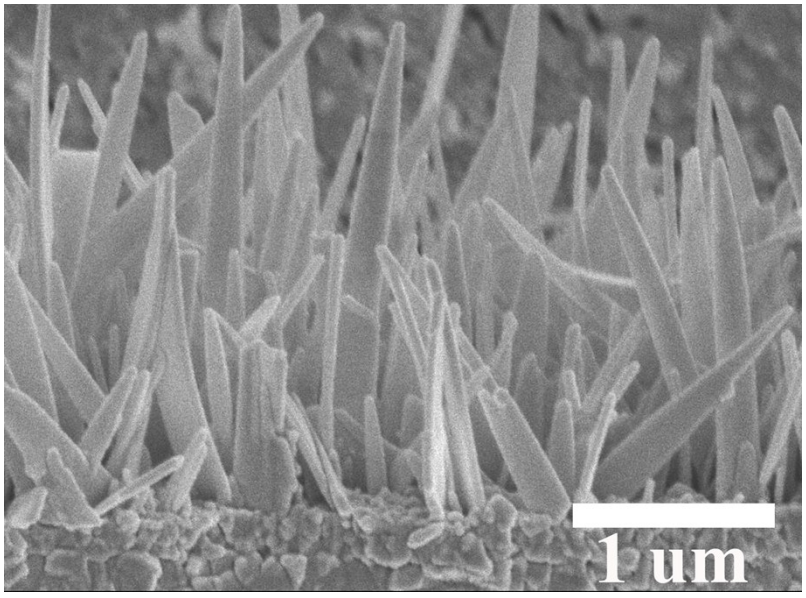

Figure S1. The side-view SEM image of the FeF_x-Fe_2O_3-Pt photoanode.

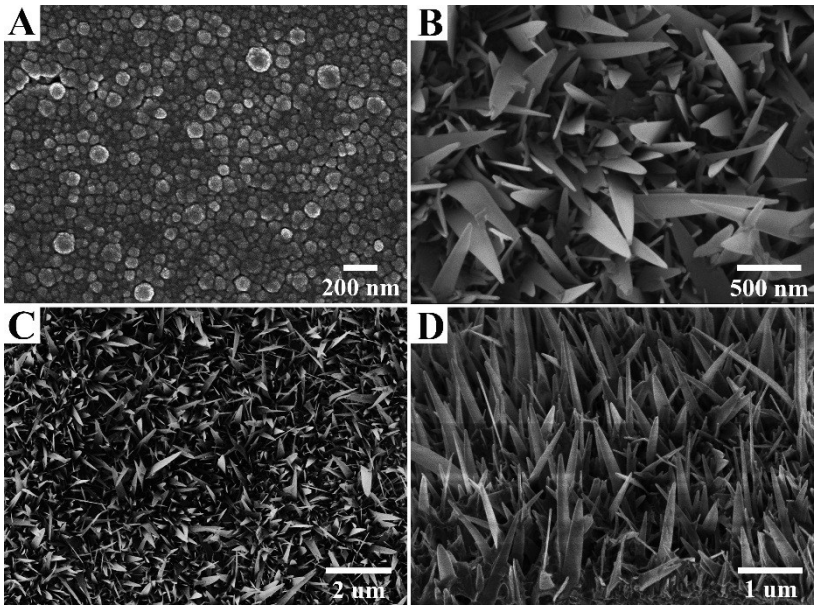

Figure S2. SEM images of Pt NPs layer (A), top (B, C) and side (D) view of Fe_2O_3-Pt photoanodes.

Additional discussion

Pt NPs were formed on the surface of Fe foils by a replacement reaction with H_2PtCl_6 precursor. As shown in Figure S2A, the as-prepared Pt NPs possess an average size of 50-100 nm.

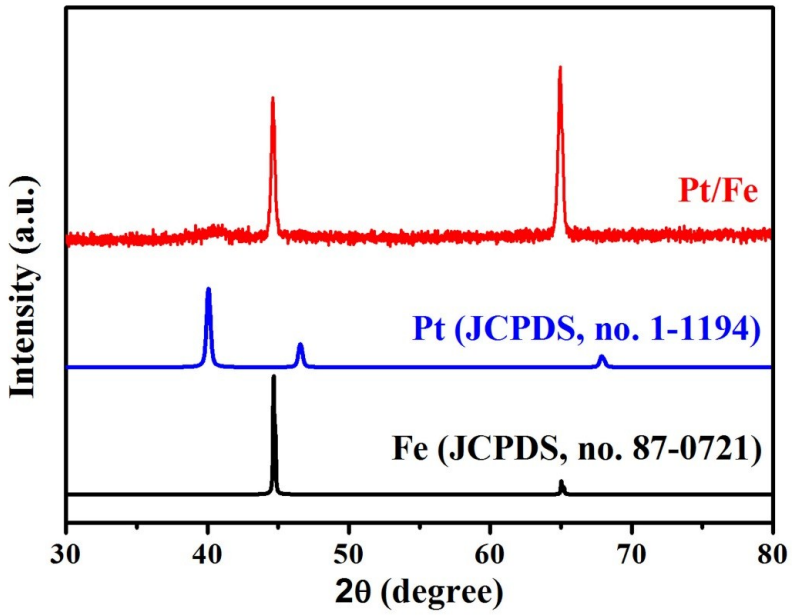

Figure S3. XRD pattern of Pt/Fe substrate.

Additional discussion

To confirm the successful formation of Pt NPs on Fe substrate, XRD pattern of Pt/Fe sample was measured. In Figure S3, a weak diffraction peak at 40° could be indexed to the standard card (JCPDS, no. 1-1194) of Pt.[3] This result reveals the existence of Pt NPs on Fe substrate.

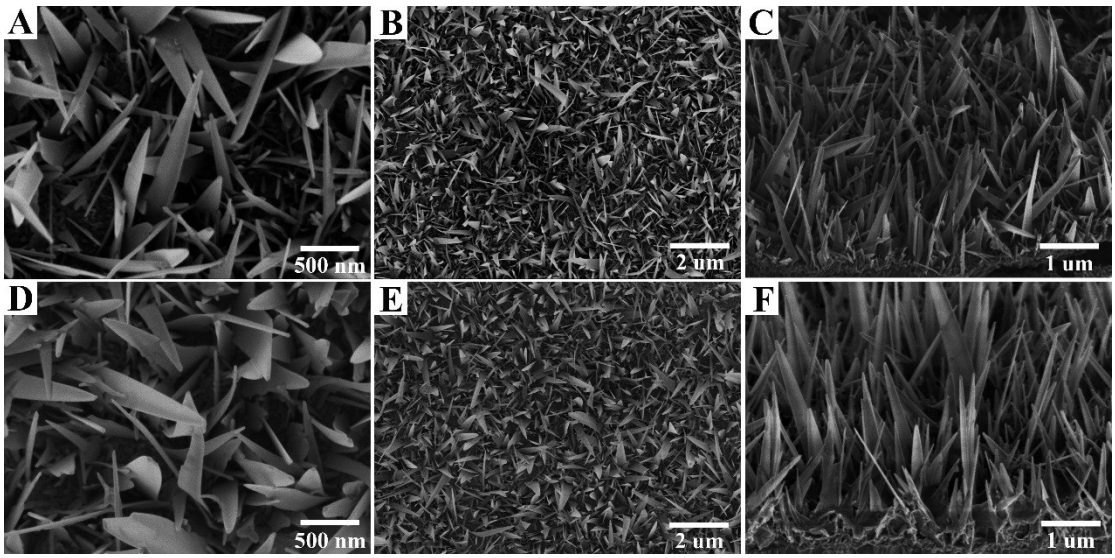

Figure S4. SEM images of top (A, B) and side (C) view for Fe_2O_3 photoanodes, and top (D, E) and side (F) view for FeF_x-Fe_2O_3 photoanodes.

Additional discussion

Figure S4 shows the SEM images of Fe_2O_3 and FeF_x-Fe_2O_3 nanoflake arrays grown on Fe substrate. The deposition of Pt NPs and *in-situ* growth of FeF_x ultrathin nanolayers have no evident damage on the flake-like structure.

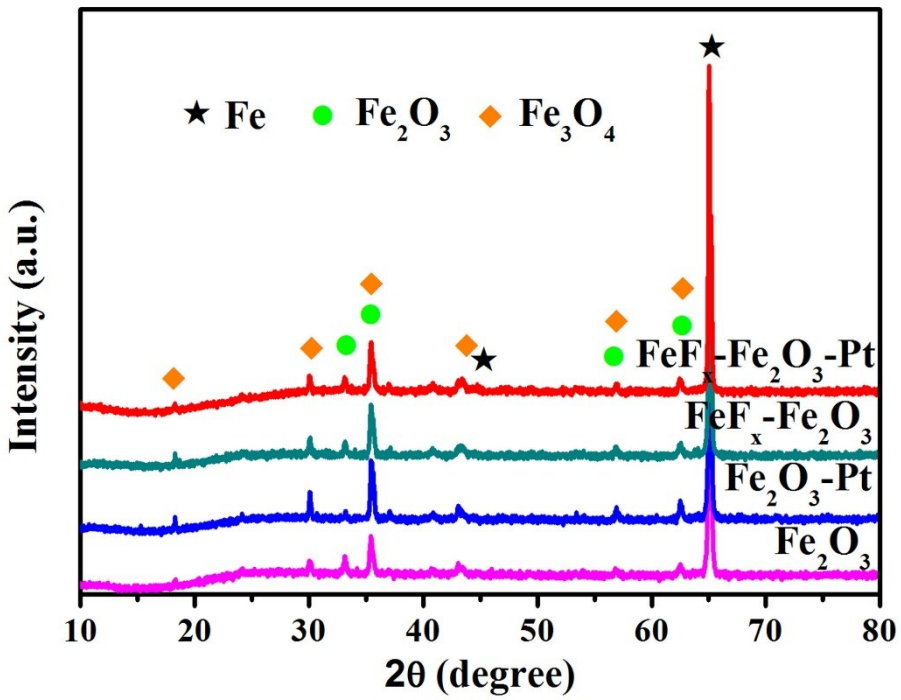

Figure S5. XRD pattern of Fe_2O_3, Fe_2O_3-Pt, FeF_x-Fe_2O_3 and FeF_x-Fe_2O_3-Pt photoanodes.

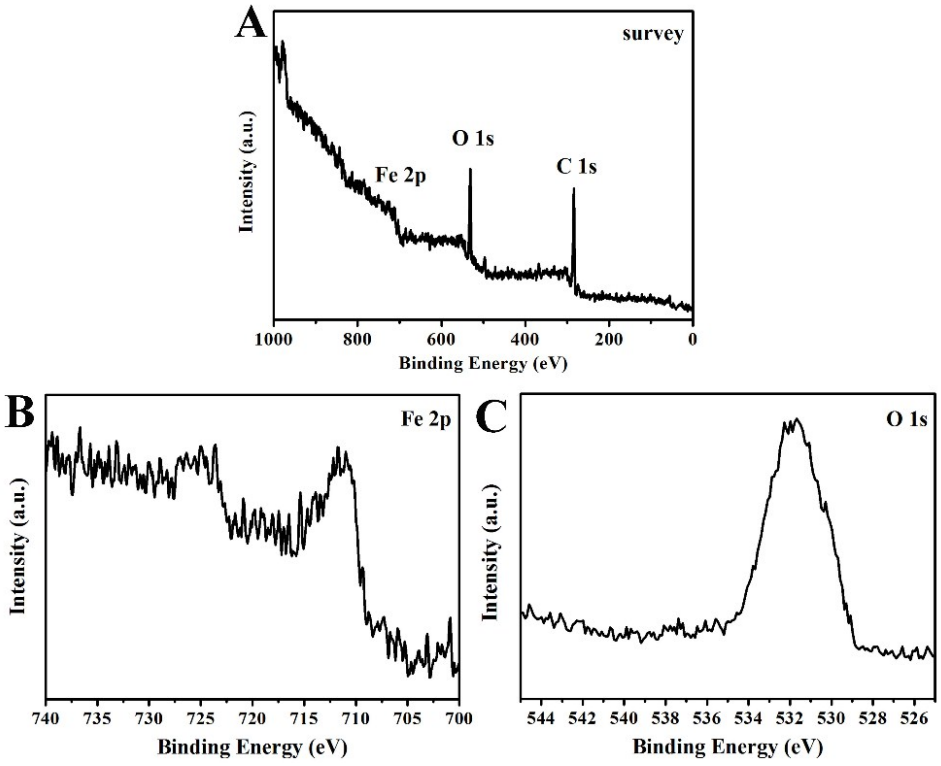

Figure S6. XPS spectra of FeF_x-Fe_2O_3-Pt photoanode.

Additional discussion

Except for the XPS spectra of F1s (Figure 2B), the survey, Fe 2p and O 1s signals were showed in Figure S6. This result shows that the as-prepared sample only contains Fe, O and F elements without other impurities.

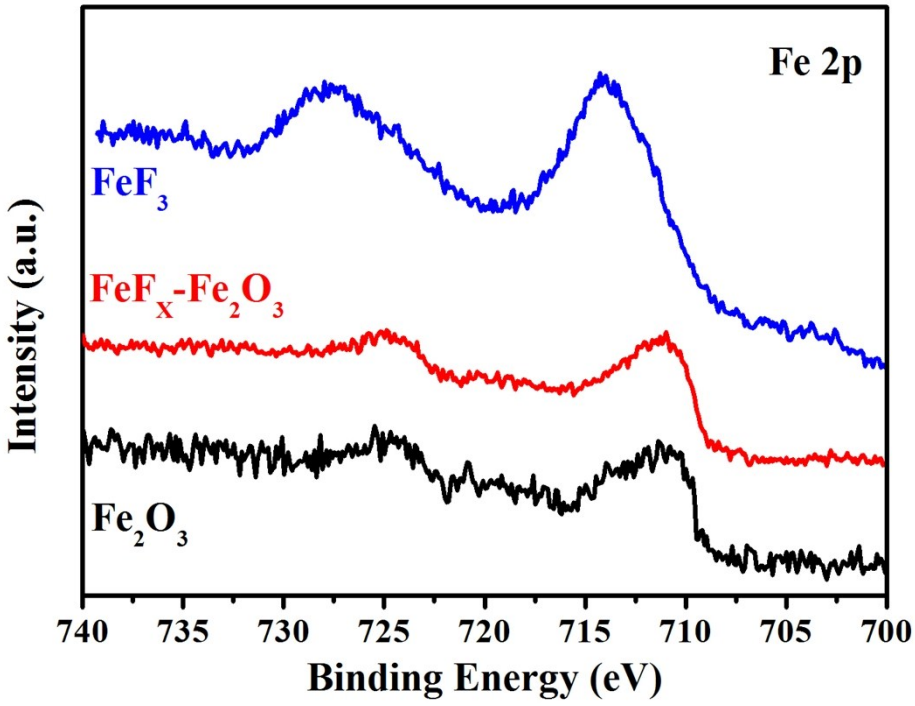

Figure S7. The Fe XPS spectra of FeF_x-Fe_2O_3, Fe_2O_3, and FeF_3 samples.

Additional discussion

The Fe XPS spectra of FeF_x-Fe_2O_3, Fe_2O_3, and FeF_3 have been compared in Figure S7. It can be clearly seen that the binding energy (BE) of Fe 2p peaks in FeF_3 is much higher than that of both Fe_2O_3 and FeF_x-Fe_2O_3 samples. However, no obvious change could be detected in Fe_2O_3 and FeF_x-Fe_2O_3, which may be resulted from the ultrathin thickness and very low amount of FeF_x nanofilms formed on the Fe_2O_3 nanoflakes after the fluorination process.

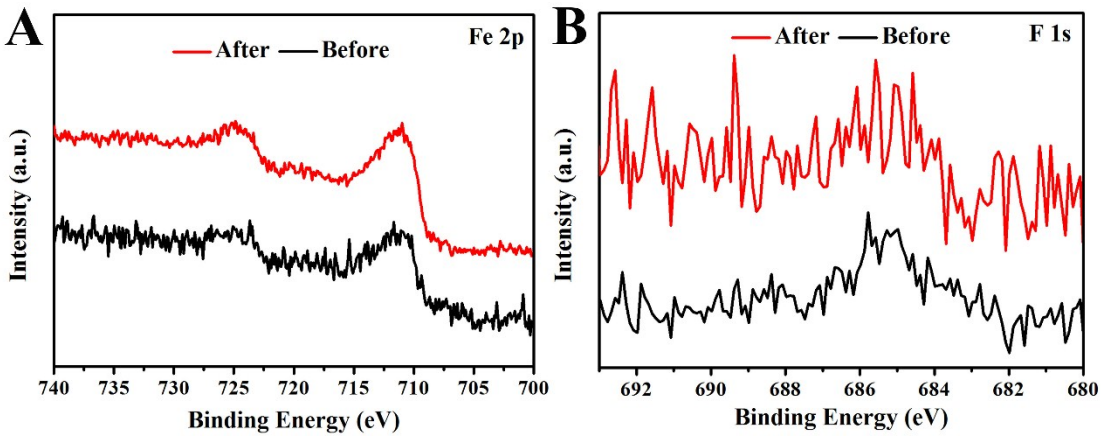

Figure S8. XPS spectra of Fe 2p and F 1s signal of FeF_x-Fe_2O_3 before and after the PEC measurements.

Additional discussion

After the PEC measurements, the chemical compositions of FeF_x ultrathin films have also been studied by XPS and compared with the fresh samples (Figure S8). It can be found that no evident changes of Fe 2p and F 1s peaks could be detected in FeF_x cocatalysts before and after the PEC measurements. Thereby, the FeF_x ultrathin films exhibit the relatively high chemical-stability during the PEC water splitting process, which may be due to their *in-situ* growth on the surfaces of Fe_2O_3 nanoflakes.[4]

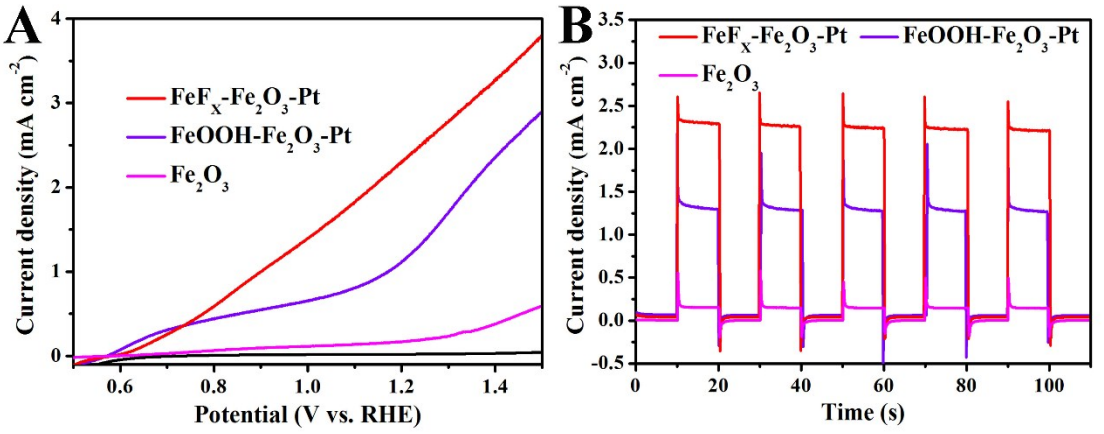

Figure S9. (A) J-V curves and (B) transient photocurrent responses under chopped illumination at 1.23 V_{RHE}.

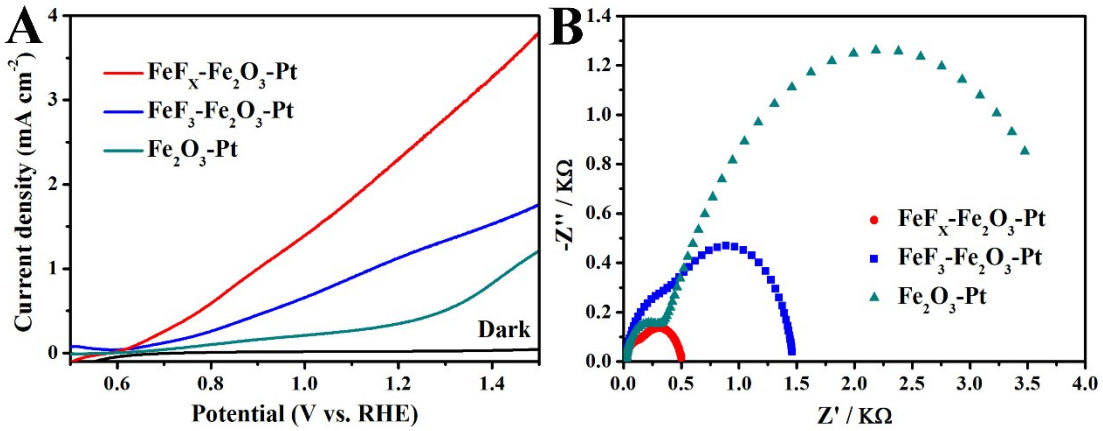

Figure S10. (A) J-V curves, and EIS Nyquist plots of Fe_2O_3-Pt, FeF_3-Fe_2O_3-Pt and FeF_x-Fe_2O_3-Pt photoanodes.

Additional discussion

To verity the merit of *in-situ* growth technology, the as-prepared FeF_3 ethanol solution was dropped on Fe_2O_3-Pt photoanodes. The photocurrent density of 1.2 mA cm^{-2} at 1.23 V_{RHE} can be obtained for the FeF_3-Fe_2O_3-Pt photoanodes (Figure S10). This comparative result suggests that the elimination of hetero-junction between anode/OER cocatalyst are beneficial to the interfacial transfer of holes.

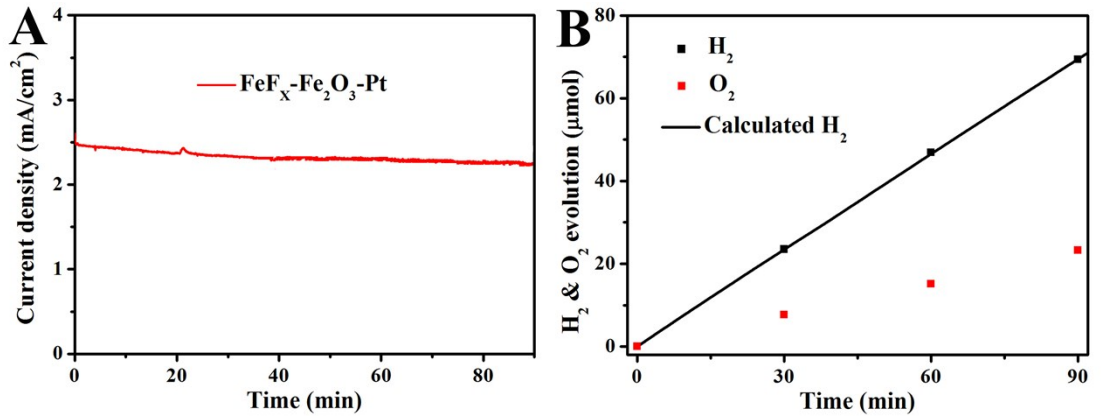

Figure S11. (A) photocurrent density versus time and (B) gas evolution from PEC water splitting of FeF_x-Fe_2O_3-Pt photoanode at 1.23 V_{RHE} under AM 1.5 G illumination in a 1.0 M KOH electrolyte.

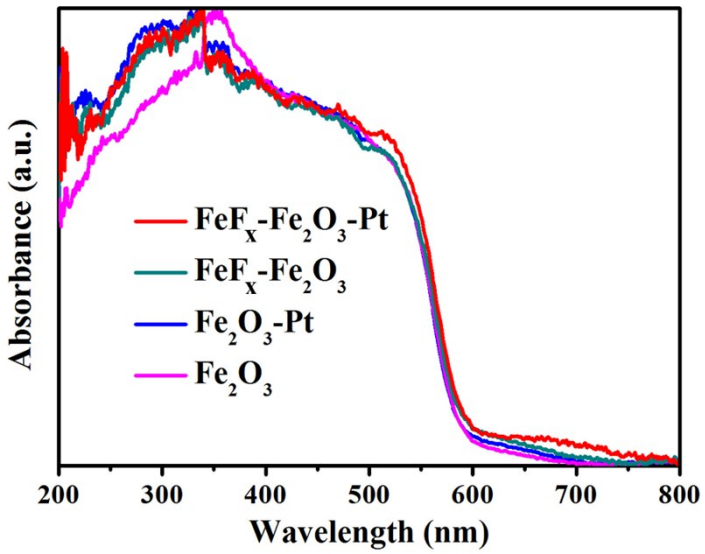

Figure S12. UV–vis spectra of Fe_2O_3, Fe_2O_3-Pt, FeF_x-Fe_2O_3 and FeF_x-Fe_2O_3-Pt photoanodes.

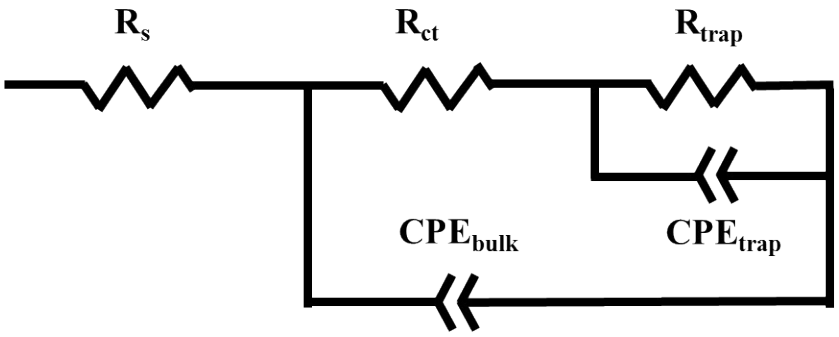

Figure S13. The equivalent circuit model used to fit the impedance data.

Additional discussion

In the equivalent circuit model, R_s represents the series resistances in the electrochemical cell, R_{ct} is the resistances in the Fe_2O_3, R_{trap} is the resistances at semiconductor/electrolyte interface, CPE_{bulk} represents the capacitance in the depletion layer of semiconductor, and CPE_{trap} is the capacitance at the surface of semiconductor.

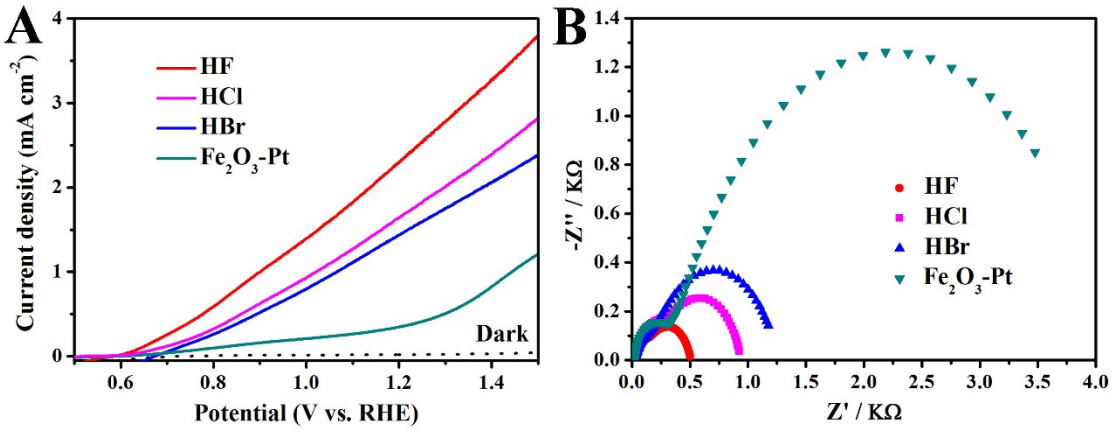

Figure S14. (A) J-V curves, and EIS Nyquist plots of Fe_2O_3-Pt photoanodes with/without dilute hydrogen fluoride, hydrochloric acid and Hydrobromic acid solution treatment.

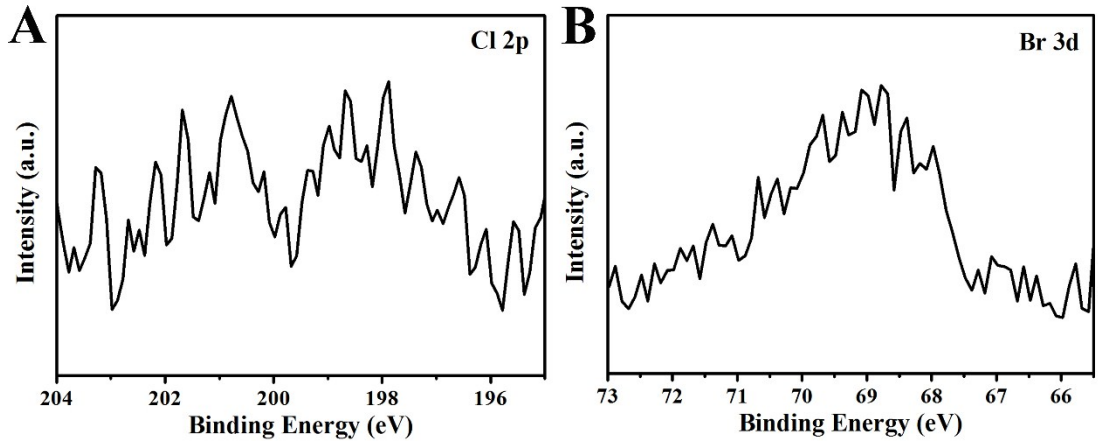

Figure S15. XPS spectra of Cl 2p and Br 3d signals of Fe_2O_3-Pt photoanodes with dilute hydrochloric acid and Hydrobromic acid solution treatment.

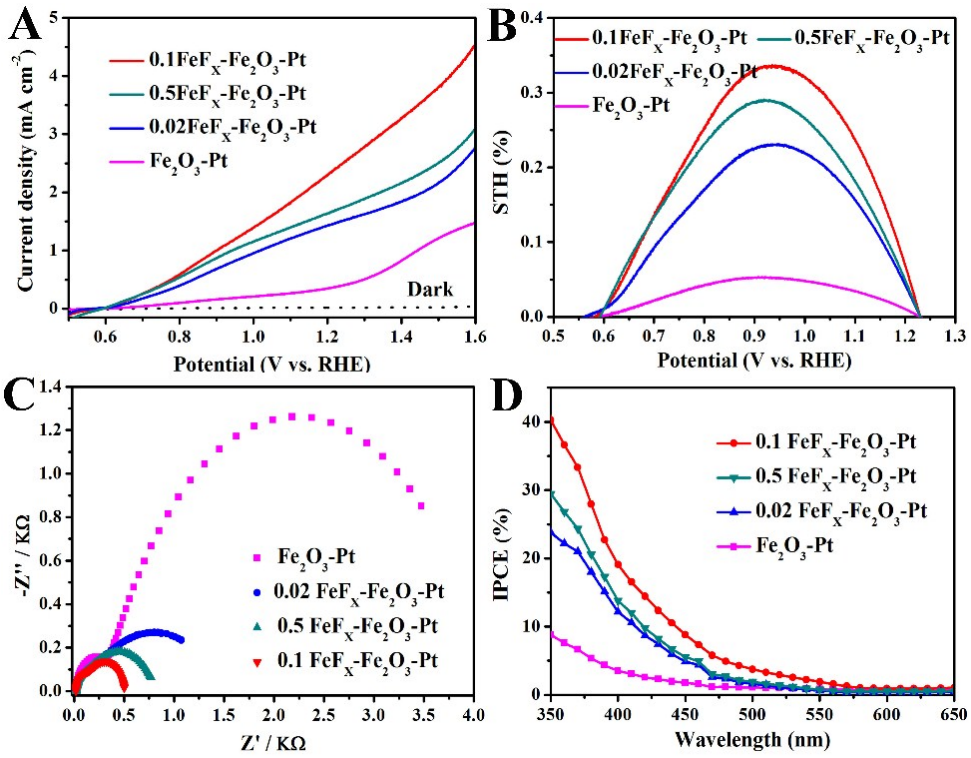

Figure S16. (A) J-V curves; (B) Photoconversion efficiency as a function of applied potential; (C) EIS Nyquist plots; (D) IPCE in the region 350-650 nm at a bias of 1.23 V_{RHE} of Fe_2O_3-Pt, 0.02FeF_x-Fe_2O_3-Pt, 0.1FeF_x-Fe_2O_3-Pt and 0.5FeF_x-Fe_2O_3-Pt photoanodes measured in 1 M KOH solution under AM 1.5 G illumination (100 mW cm^{-2}).

Additional discussion

To investigate the effect of the size and thickness of FeF_x layer in PEC performance, we immersed the Fe_2O_3 or Fe_2O_3-Pt photoanodes in the various solution. As shown in Figure S16, with increasing or decreasing the thickness of FeF_x layer by adjusting the concentrations of HF solution, the PEC performances of as-obtained samples have been both decreased. In detail, when fluoride solution contains too few F^-, the surface of nanoflakes would be partly fluoride, which directly effects the hole transfer on the surface of catalyst. In addition, with the excess F^-, the nanoflake structure would suffer from corrosion, and then the light absorption capacity of photoanodes would be weakened.

Table S1. The fitting results using the equivalent model for EIS measurements

Photoelectrodes	R(Ω)			CPE (F)	
	R_s	R_{ct}	R_{trap}	CPE_{bulk}	CPE_{trap}
FeF_x-Fe_2O_3-Pt	18.65	161.1	328.2	1.26×10^{-5}	0.19×10^{-3}
Fe_2O_3-Pt	18.96	337.4	2582	6.13×10^{-6}	0.20×10^{-5}
Fe_2O_3	18.5	446.8	9514	4.33×10^{-6}	0.18×10^{-3}

Table S2. Photocurrent densities and IPCE of recent hematite photoelectrodes in PEC water splitting.[3-6]

Electrodes	Electrolyte	Photocurrent density ($1.23\ V_{RHE}$, AM 1.5G)	IPCE ($1.23\ V_{RHE}$, 350 nm)	Reference
NiO/P-Fe_2O_3	1 M KOH	2.08 mA cm^{-2}	38 %	5
Sn-Fe_2O_3	1 M KOH	2.2 mA cm^{-2}	27 %	6
NiOOH/Sn, Zr-Fe_2O_3	1 M NaOH	1.64 mA cm^{-2}	31 %	7
Co-Pi/P-Fe_2O_3	1 M KOH	2.0 mA cm^{-2}	25 %	8
This work	1 M KOH	2.4 mA cm^{-2}	41 %	

3. Reference

[1] L. Wang, Y. Yang, Y. Zhang, Q. Rui, B. Zhang, Z. Shen, Y. Bi, *J. Mater. Chem. A*, 2017, **5**, 17056.

[2] L. Li, Y. Yu, F. Meng, Y. Tan, R. J. Hamers, S. Jin, *Nano Lett*. 2012, **12**, 724.

[3] G. X. Lu and B. Tian, *J. Mol. Catal. (China)*, 2017, **31**, 101.

[4] Y. J. Ou, S. P. Li and Y, P, Bi, *J. Mol. Catal. (China)*, 2015, **5**, 441.

[5] Feng Li, Jing Li, Jie Zhang, Lili Gao, Xuefeng Long, Yiping Hu, Shuwen Li, Jun Jin and Jiantai Ma, *ChemSusChem*, 2018, **11**, 1.

[6] M. Y. Li, Y. Yang, Y. C. Ling, W. T. Qiu, F. X. Wang, T. Y. Liu, Y, Song, X. X. Liu, P. P. Fang, Y. X. Tong and Y. Li, *Nano Lett*. 2017, **17**, 2490.

[7] A. G. Tamirat, W. N. Su, A. A. Dubale, H. M. Chen and B. J. Hwang, *J. Mater. Chem. A*, 2015, **3**, 5949.

[8] Z. B. Luo, C. C. Li, S. S. Liu, T. Wang and J. L. Gong, *Chem. Sci.*, 2017, **8**, 91.